Toxicology in Vitro 28 (2014) 60–69

Contents lists available at SciVerse ScienceDirect

Toxicology in Vitro

journal homepage: www.elsevier.com/locate/toxinvit

# Genotoxicity evaluation of nanosized titanium dioxide, synthetic amorphous silica and multi-walled carbon nanotubes in human lymphocytes

Ana M. Tavares [a], Henriqueta Louro [a,*], Susana Antunes [a], Stephanie Quarré [b], Sophie Simar [b], Pieter-Jan De Temmerman [c], Eveline Verleysen [c], Jan Mast [c], Keld A. Jensen [d], Hannu Norppa [e], Fabrice Nesslany [b], Maria João Silva [a]

[a] Department of Human Genetics, National Institute of Health Dr. Ricardo Jorge (INSA), Av. Padre Cruz, 1649-016 Lisbon, Portugal
[b] Toxicology Laboratory of Institut Pasteur de Lille, EA 4483, 1 rue du Professeur Calmette, BP 245, 59019 Lille, France
[c] Electron Microscopy-unit, Veterinary and Agrochemical Research Centre (CODA-CERVA), Groeselenberg 99, 1180 Brussels, Belgium
[d] Danish Centre for Nanosafety National Research Centre for the Working Environment, Lerso Parkallé 105, Copenhagen DK-2100, Denmark
[e] Nanosafety Research Center, Finnish Institute of Occupational Health, FI-00250 Helsinki, Finland

ARTICLE INFO

*Article history:*
Received 20 November 2012
Accepted 18 June 2013
Available online 27 June 2013

*Keywords:*
Titanium dioxide nanomaterials
Synthetic amorphous silica nanomaterials
Multiwalled carbon nanotubes
Morphology and size
Primary human lymphocytes
Micronucleus assay

ABSTRACT

Toxicological characterization of manufactured nanomaterials (NMs) is essential for safety assessment, while keeping pace with innovation from their development and application in consumer products. The specific physicochemical properties of NMs, including size and morphology, might influence their toxicity and have impact on human health. The present work aimed to evaluate the genotoxicity of nanosized titanium dioxide ($TiO_2$), synthetic amorphous silica (SAS) and multiwalled carbon nanotubes (MWCNTs), in human lymphocytes. The morphology and size of those NMs were characterized by transmission electron microscopy, while the hydrodynamic particle size-distributions were determined by dynamic light scattering. Using a standardized procedure to ensure the dispersion of the NMs and the cytokinesis-block micronucleus assay (without metabolic activation), we observed significant increases in the frequencies of micronucleated binucleated cells (MNBCs) for some $TiO_2$ NMs and for two MWCNTs, although no clear dose–response relationships could be disclosed. In contrast, all forms of SAS analyzed in this study were unable to induce micronuclei. The present findings increase the weight of evidence towards a genotoxic effect of some forms of $TiO_2$ and some MWCNTs. Regarding safety assessment, the differential genotoxicity observed for closely related NMs highlights the importance of investigating the toxic potential of each NM individually, instead of assuming a common mechanism and equal genotoxic effects for a set of similar NMs.



## 1. Introduction

Nanomaterials have specific properties, such as small size and high surface area/mass ratio that render them attractive for many applications in consumer products and biomedicine. The wide applicability of manufactured nanomaterials (NMs) has led to an increased risk of human exposure and environmental dissemination. The same properties that make NMs technologically interesting may also imply a higher toxicity in biological systems and in humans, comparatively to the bulk materials (Oberdörster, 2010), raising questions about their safety for public health. In particular, it has been suggested that NMs may be genotoxic either due to a direct interaction with DNA or to indirect mechanisms of DNA damage (reviewed in Singh et al., 2009).

Titanium dioxide ($TiO_2$), zinc oxide (ZnO), synthetic amorphous silica nanoparticles (SAS), and multi-walled carbon nanotubes (MWCNTs) are among the most commonly utilized NMs. $TiO_2$, ZnO, and SAS have widely been used in a diversity of products including cosmetics, pharmaceuticals, food, and inks, and MWCNTs have been applied as structural composites, in energy appliances and electronics (Wijnhoven et al., 2009). Although many studies have tried to address the potential genotoxicity of some of these NMs, contradictory results have been reported. For example, conflicting results have been described for the genotoxicity of nanosized $TiO_2$ in several cellular systems (reviewed in Sycheva et al., 2011). In human lymphocytes, contradictory results have been obtained for $TiO_2$ nanoparticles in the comet assay (Ghosh et al., 2010; Hackenberg et al., 2011a; Kang et al., 2008), while the few

* Corresponding author. Tel.: +351 217 526 423; fax: +351 217 526 410.
*E-mail address:* henriqueta.louro@insa.min-saude.pt (H. Louro).

0887-2333/$ - see front matter © 2013 Elsevier Ltd. All rights reserved.
http://dx.doi.org/10.1016/j.tiv.2013.06.009

lymphocyte studies available on nanosized or bulk $TiO_2$ in the micronucleus and the chromosomal aberration assays have been positive (Catalán et al., 2012; Kang et al., 2008; Türkez and Geyikoglu, 2007). Various types of SAS, have given both negative and positive results in the *in vitro* micronucleus, comet and mutation assays with various cell systems (Downs et al., 2012; Guidi et al., 2013; Gonzalez et al., 2010; Park et al., 2011; Lankoff et al., 2012; Uboldi et al., 2012). Negative results were reported in one study on the chromosomal aberration assay with human lymphocytes (Lankoff et al., 2012). Discrepant results have also been reported for MWCNTs, either showing induction of DNA damage, gene mutations, micronuclei, and chromosomal aberrations in different types of cells (Cveticanin et al., 2010; Di Giorgio et al., 2011; Guo et al., 2011; Lindberg et al., 2009; Muller et al., 2008; Zhu et al., 2007) or no such effects (Asakura et al., 2010; Szendi and Varga, 2008). The inconsistent results found in the literature may be related to differences in the physicochemical properties of the NMs studied and to other variables inherent to the test systems and exposure conditions, including dispersion of the nanoparticles. Firstly, even NMs with the same chemistry can greatly differ by size, surface area, shape, stability, rigidness, coating and electrical charge; these characteristics affect the possible interactions with living cells or tissues and some may be central to determine genotoxicity. Secondly, experimental conditions related to the NMs dispersion in aqueous solutions, possibly affecting subsequent agglomeration or aggregation may interfere in unpredictable ways with the results obtained. Therefore, the use of standardized methods has been recommended to allow comparisons of the results obtained for a given NM among laboratories and to compare the genotoxic potential of several NMs (Oesch and Landsiedel, 2012). In addition, testing of well characterized NMs has been recognized to be crucial to evaluate the efficiency of the commonly used genotoxicity assays (e.g., micronucleus assay) in assessing the genotoxic effect of NMs and their impact on human health (Joint Research Center, 2011).

In line with this view, the objective of the present work was to assess the potential genotoxic effects of a panel of NMs in human lymphocytes, contributing to their safety evaluation. The NMs selected were representative of three classes that are widely used in consumer products and medicine: $TiO_2$, SAS and MWCNTs. Furthermore, a standardized protocol, developed to minimize agglomeration of the nanosized particles (Jensen et al., 2011) was followed to disperse the NMs before cells exposure. The *in vitro* micronucleus assay in human lymphocytes, which is a sensitive indicator of chromosome structural and numerical changes, was selected because it is a validated method accepted for regulatory purposes (OECD, 2010).

## 2. Materials and methods

### 2.1. Manufactured nanomaterials

All selected NMs, except two MWCNTs, were provided by the Joint Research Centre (JRC; NM codes starting with 'NM'). The NMs were prepared under Good Laboratory Practices (GLP), allowing their application as international benchmarks (http://ihcp.jrc.ec.europa.eu/our_activities/nanotechnology/nanomaterials-repository). The nanomaterials coded as NRCWE-006 (Mitsui&Co., Ltd., Ibaraki, Japan) and NRCWE-007 (Cheap Tubes Inc., Brattleboro, VT, USA) were provided as sub-samples by the National Research Centre for the Working and Environment (NRCWE). Four nanosized $TiO_2$ (NM-102, NM-103, NM-104 and NM-105), four nanosized SAS (NM-200, NM-201, NM-202 and NM-203), and six different MWCNTs (NM-400, NM-401, NM-402, NM-403, NRCWE-006 and NRCWE-007) were selected. Zinc oxide (NM-110, Joint Research Centre) was assessed as a possible nanosized positive control since ZnO NMs have been shown to be genotoxic in human cells (Corradi et al., 2012; Gopalan et al., 2009; Hackenberg et al., 2011b; Wahab et al., 2011).

### 2.2. Dispersion in aqueous medium

A 2.56 mg/ml stock dispersion of each NM was prepared by prewetting powder in 0.5 vol% ethanol (96%) followed by addition of sterile-filtered 0.05 wt% BSA-water and dispersion by 16 min of probe sonication of the sample, cooled in an ice-water bath (Jensen et al., 2011). According to the protocol, the batch dispersions are metastable and, for most samples, maintained for at least 1 h.

### 2.3. Characterization of nanomaterials

The morphology and size of nanoparticles in the stock dispersion was determined by transmission electron microscopy (TEM). Samples for TEM were prepared by the grid on drop method, using pioloform- and carbon-coated, 400 mesh copper grids (Agar Scientific, Essex, England) that were pretreated with 1% Alcian blue (Fluka, Buchs, Switzerland) to increase hydrophilicity, as described in Mast and Demeestere (2009). The electron micrographs were recorded as described by De Temmerman et al. (2012). The samples were imaged in bright field mode using a Tecnai Spirit TEM (FEI, Eindhoven, the Netherlands) with Biotwin lens configuration operating at 120 kV. Micrographs were recorded using a $4 * 4$ K CCD camera (Eagle, FEI), at a magnification of 30 000×, with a pixel size of 0.375 nm-and a field of view of 1.53 μm by 1.53 μm. For NM-401 and NRCWE-006 a magnification of 6800×, with a pixel size of 1.6 nm-and a field of view of 6.58 μm by 6.58 μm was used. To determine the characteristic size and shape of the primary particles of $TiO_2$, SAS and ZnO the feret diameters, feret maximum and feret minimum, were measured. Furthermore, for fibrous particles such as MWCNTs, the thickness and geodesic length were measured as described (ISO 9276-6, 2008). The feret maximum, feret minimum and thickness were manually measured using the iTEM software (Olympus, Münster, Germany) using the arbitrary line tool. The geodesic length was manually measured using the polyline tool. The aspect ratio was calculated as the ratio between the feret maximum and feret minimum for $TiO_2$, SAS and ZnO and as the ratio between the geodesic length and the thickness for the MWCNTs. The geometric mean and geometric standard deviation of the mean were calculated as described (ISO, 2004).

### 2.4. Characterization of the batch dispersions and exposure media

Hydrodynamic particle size-distributions were determined in the batch dispersions by dynamic light scattering (DLS) at measured viscosities based on the photon correlation spectroscopy. Viscosities of the dispersions were determined using a AND Vibro Viscometer Model SV-10 (A&D Company, Ltd.). The viscosity was measured in 10 ml flow-cell cuvettes at 25 °C, corresponding to the analytical conditions for DLS analysis. The temperature was ensured using recirculated water conditioned in Gant thermostatic water-bath. The viscosity of the batch dispersions were 0.99 cP for NM-102, NM-200, NM-201and NM-203, and 1.00 cP for NM-103, NM-104, NM-105, NM-202, NM-401, NRCWE-006 and NRCWE-007. High viscosities were found for NM-400 (2.98 cP), NM-402 (2.31 cP), and NM-403 (1.76 cP).

DLS analysis was performed using a Malvern Nano ZS (Malvern Inc., UK). App. 0.7–1.0 ml suspension was entered in disposable standard 1 ml polystyrene cuvette using polymer pipette tips and started to be analyzed within 5–10 min after preparation. Thermal equilibrium time was set to 2 min, and the data was obtained using specific optical parameters (refractive indices, $R_i$ and Absorption, $R_{abs}$) for the different samples ($R_i = 2.903$ and $R_{abs} = 0.1$ for rutile;

$R_i$ = 2.49 and $R_{abs}$ = 0.1 for anatase; $R_i$ = 1.544 and $R_{abs}$ = 0.2 for SAS; $R_i$ = 2.02 and $R_{abs}$ = 2.0 for MWCNT; and $R_i$ = 1.33 and $R_{abs}$ = 0 for the cell medium). Each size spectra is the average of six individual DLS analysis conducted using automatic optimization of analytical conditions and data treatment by general purpose size-analysis. For NM-403, however, the size-distribution data were averaged based on 12 first analyses due to variable solutions to the photon correlation spectroscopy data.

Overall agglomeration/de-agglomeration and sedimentation of the suspended nanomaterials in RPMI 1640 cell media added 15–20% w/v fetal calf serum, as used in the in micronucleus assay described below, was also investigated using the DLS technique. All studies were completed at 0.256 mg/ml made by simply adding 0.1 ml batch dispersion to 0.9 ml serum-completed RPMI in a polystyrene DLS cuvette. Mixing and measurements started within ca. 10–15 min after completion of the probe-sonication of the batch dispersion and lasted for ca. 6 h to study the dispersion fate in the *in vitro* system until addition of cytochalasin B (see protocol for the micronucleus assay below). The first, 4–6 DLS measurements were made using automatic optimization of the measurement conditions. This was followed by measurements at each 30 min interval until ca. 6 h using the measurement depth and laser attenuation in the initial 4–6 measurements. This allows use of the variation in Zeta-size (Zeta-ave) and change in relative laser scattering intensity ($I/I_o$) with time to qualitatively assess agglomeration effects and sedimentation fraction of material sedimented from suspension. $I_o$ is the scattered intensity in the first measurement and $I$ is the intensity in the specific measurement. For the analysis, we used the material and media optical data mentioned above and measured viscosities of 1.0268 and 1.0428 cP for RPMI with 15% and 20% fetal calf serum, respectively. All tests were conducted at 37°C to mimic best possible the *in vitro* test conditions.

### 2.5. Exposure of cells and in vitro micronucleus assay in human lymphocytes

Since preliminary data indicated that none of the NMs under study was strongly cytotoxic, the highest concentration of each NM selected for the *in vitro* micronucleus assay was limited by its dispersibility, i.e. the maximum concentration that could be homogenously dispersed in BSA/water (2.56 mg/ml for the majority of NMs). Also, the highest percentage of the batch dispersion (10%) that could be added to the cultures without interference with the normal cell proliferation capacity was taken into account, leading to a top concentration of 256 μg/ml. Nevertheless, whenever the quality of the dispersion appeared satisfactory, NMs were tested up to the maximum concentration that allowed an adequate microscopic analysis, i.e., that did not cover cells preventing micronucleus scoring (e.g., NM-202 and NM-203 were tested up to 1250 μg/ml).

Blood samples were collected from non-smoking healthy donors (4 males and 6 females), less than 35 years of age, with no recent exposures to genotoxicants or ionizing radiation and were individually used in several experiments carried out to assess the genotoxicity of the fourteen NMs under study. The *in vitro* micronucleus assay in human peripheral lymphocytes was performed following the general principles of OECD Guideline 487 (2010). Although a short and a long treatment are recommended, only a long-term continuous treatment (30 h) was used because it is the most informative, taking into account that the uptake of the NMs by the cell has been shown to be time-dependent (Jin et al., 2007). Moreover, an exposure during mitosis has also the advantage of allowing the contact between the NMs and the chromatin, which might be especially important for those NMs that do not enter the nucleus (Gonzalez et al., 2011).

Briefly, blood samples (500 μl) from each donor were cultured in RPMI-1640 medium (Gibco-Invitrogen, Carlsbad, CA) supplemented with fetal calf serum (15–20%, Gibco-Invitrogen) and phytohemaglutinin A (PHA, 2.5%, Gibco-Invitrogen), for 38 h at 37 °C. At this time point, the exponentially growing cells were exposed to several concentrations of a NM, 6 h prior to cytochalasin B addition (Sigma–Aldrich, St. Louis, MO) to avoid interference of this chemical with NMs uptake, and the cultures were incubated for additional 24 h, allowing the majority of stimulated lymphocytes to complete 1.5–2 cell cycles as previously shown (Silva et al., 1994). No pH changes were noted following NMs addition, independently of the concentration. At the end of the exposure period lymphocytes were harvested by treatment with a hypotonic solution (KCl 0.1 M), followed by fixation (methanol:acetic acid, 3:1). Cells were immediately dropped onto microscope slides and after air-drying they were stained with Giemsa (Merck, Darmstadt, Germany). All experiments included cells treatment with mitomycin C (MMC; Sigma–Aldrich), at 0.075 or 0.167 μg/ml, as the positive control and with the dispersion medium (BSA/water), as the vehicle control; NM-110 (64 μg/ml) was used as a candidate positive control. For each treatment condition, at least two replicate cultures were used. Coded slides were "blind" analyzed under a bright field microscope and micronuclei were scored in, at least, 2000 binucleate cells and 1000 mononucleate cells from 2 independent cultures. The proportion of mono- (MC), bi- (BC) or multinucleate cells (MTC) was determined in a total of 1000 cells and the cytokinesis-block proliferation index (CBPI) was calculated as follows (OECD, 2010):

$$\mathrm{CBPI} = (\mathrm{MC} + 2\mathrm{BC} + 3\mathrm{MTC})/\text{Total cells}$$

The replication Index (RI) of NMs-treated cultures, relative to vehicle control cultures, was also calculated by the formula:

$$\mathrm{RI} = 100 \times [(\mathrm{BC} + 2\mathrm{MTC})/\text{Total cells})]_{\text{treated}} / [(\mathrm{BC} + 2\mathrm{MTC})/\text{Total cells})]_{\text{control}}$$

Two-sided Fisher's exact test was applied to compare the frequency of micronucleated cells between NM-treated and vehicle-treated cultures. CBPI and RI data were analyzed using one-way ANOVA or Kruskal–Wallis test. In addition, the existence of a dose-response relationship either for the frequency of micronucleated cells or for CBPI was explored by regression analysis.

## 3. Results

### 3.1. Characterization of nanomaterials

The TEM analyses (Tables 1 and 2) confirm that the examined materials qualify as NM according to the EC definition (EC, 2012). The size distributions of the agglomerates of $TiO_2$ and SAS NMs in the stock dispersion were similar. They are narrower than the distribution of the NM-110 control. The primary particles of the $TiO_2$, ZnO and SAS showed a relatively high sphericity (Krumbein and Sloss, 1963). In agreement with Singh et al. (2011), the primary particles of the $TiO_2$ and ZnO NMs were polyhedral, while the primary particles of the SAS were ellipsoidal, forming fractal-like aggregates. MWCNTs qualify as nanofibers, according to ISO (ISO, 2008). Sonication of the MWCNTs unraveled the 1 to 5 μm ball-like agglomerates to open net-like structures of partially entangled MWCNTs. The number of walls of the flexible MWCNTs, NM-400, NM-402, NM-403 and NRCWE-007, was lower than that of the rigid NM-401 and NRCWE-006. The tips of the latter tubes tended to form knot-like structures.

### 3.2. Characterization of the batch dispersions

Conversion of the photon correlation spectra obtained by DLS to hydrodynamic number size-distributions showed that all $TiO_2$ NMs had a primary peak in the range of 78.8 (NM-103) and 122.4 nm

**Table 1**
Geometric mean Feret's minimum and maximum diameter, aspect ratio of primary particles and boundaries of typical aggregate/agglomerate size for various $TiO_2$, ZnO and $SiO_2$ nanoparticles.

| Nanomaterial | | Phase (and other information)[a] | Impurities/coatings (surface modification) | Specific surface area ($m^2/g$) [a] | Primary particles | | | | Aggregates/agglomerates[d] | | |
|---|---|---|---|---|---|---|---|---|---|---|---|
| | | | | | Feret Min ± SD (nm)[b] | Feret Max ± SD (nm)[b] | Aspect ratio ± SD[b] | $N$[c] | 25% (nm) | Median (nm) | 75% (nm) |
| $TiO_2$ | NM-102 | Anatase | – | 90 | 20.8 ± 1.6 | 33.0 ± 1.5 | 1.5 ± 1.3 | 59 | 43 | 54 | 72 |
| | NM-103 | Rutile (hydrophobic) | Dimethicone 2% [e] | 60 | 21.9 ± 1.4 | 37.9 ± 1.6 | 1.7 ± 1.3 | 40 | 33 | 67 | 129 |
| | NM-104 | Rutile (hydrophilic) | Glycerine[e] | 60 | 19.0 ± 1.5 | 25.8 ± 1.4 | 1.4 ± 1.3 | 47 | 33 | 60 | 112 |
| | NM-105 | Rutile-anatase (15–85%) | None[e] | 61 | 20.0 ± 1.3 | 29.6 ± 1.3 | 1.4 ± 1.2 | 42 | 55 | 90 | 144 |
| ZnO | NM-110[f] | Uncoated | – | 13 | 37.1 ± 1.3 | 56.3 ± 1.4 | 1.4 ± 1.2 | 33 | 74 | 149 | 237 |
| SAS | NM-200 | Amorphous (PR-A-02) | – | 230 | 14.5 ± 1.4 | 23.1 ± 1.4 | 1.6 ± 1.4 | 54 | 40 | 62 | 102 |
| | NM-201 | Amorphous (PR-B-01) | – | 160 | 12.7 ± 1.3 | 15.4 ± 1.4 | 1.4 ± 1.3 | 42 | 56 | 83 | 152 |
| | NM-202 | Amorphous (PY-AB-03) | – | 200 | 10.4 ± 1.5 | 13.5 ± 1.5 | 1.5 ± 1.3 | 44 | 42 | 74 | 127 |
| | NM-203 | Amorphous (PY-A-04) | – | 226 | 16.0 ± 1.3 | 24.0 ± 1.4 | 1.5 ± 1.3 | 56 | 51 | 86 | 143 |

[a] Information provided by Joint Research Center (http://ihcp.jrc.ec.europa.eu/our_activities/nanotechnology/nanomaterials-repository/list_materials_JRC_rep_oct_2011.pdf).
[b] Geometric mean with its geometric standard deviation, determined by transmission electron microscopy.
[c] Number of measured primary particles.
[d] Boundaries of typical aggregate and agglomerate size (25% and 75% percentiles of the mean diameter), determined by transmission electron microscopy.
[e] Malhi, 2012.
[f] Detailed information on NM-110 has been published (Singh et al., 2011).

**Table 2**
Geometric mean thickness, geodesic length, and aspect ratio of multi-walled carbon nanotubes.

| Multi-walled carbon nanotubes | Specific surface area ($m^2/g$)[a] | Thickness ± SD (nm) | Geodesic length ± SD (nm) | Aspect ratio ± SD | $N$[b] |
|---|---|---|---|---|---|
| NM-400 | 280 | 10.8 ± 1.3 | 726.3 ± 1.8 | 67.3 ± 1.8 | 20 |
| NM-401 | 300 | 62.8 ± 1.4 | 3366.4 ± 1.9 | 53.6 ± 2.0 | 43 |
| NM-402 | 250 | 10.7 ± 1.3 | 1141.3 ± 2.0 | 107.1 ± 1.9 | 20 |
| NM-403 | – | 11.1 ± 1.5 | 394.3 ± 1.6 | 35.6 ± 1.8 | 50 |
| NRCWE-006 | 24–28 | 69.4 ± 1.4 | 4423.6 ± 2.3 | 63.7 ± 2.4 | 56 |
| NRCWE-007 | 233 | 15.3 ± 1.5 | 368.7 ± 2.0 | 24.1 ± 1.9 | 50 |

[a] Information provided by manufacturer or the Joint Research Center (http://ihcp.jrc.ec.europa.eu/our_activities/nanotechnology/nanomaterials-repository/list_materials_JRC_rep_oct_2011.pdf).
[b] Number of measured primary particles.

(NM-102) in the 0.05% BSA batch dispersion (Fig. 1a). NM-102 had a secondary peak at ca. 615 nm. NM-103 also showed a weak shoulder indicating a secondary peak at ca. 300 nm. The polydispersivity index (PDI) for the $TiO_2$ NM dispersions varied between 0.135 ± 0.017 (NM-105) and 0.324 ± 0.020 (NM-103).

The SAS samples all showed a primary peak around 70 nm and coarsening upwards shoulder due to detectable particles in the size-range up to ca. 500 nm size (Fig. 1b). NM-200 and NM-201 both had a wider size-distribution than NM-202 and NM-203 with a secondary peak at ca. 30 to 40 nm. The hydrodynamic size-distribution obtained for NM-200 and NM-201 were remarkably similar. The PDI for the SAS NM varied between 0.153 ± 0.027 (NM-203) and 0.313 ± 0.023 (NM-200).

The DLS analyses were also made on the MWCNT dispersions. Due to the morphological nature of MWCNTs, there is not a good understanding of what the size-spectra in DLS analyses represent. However, as in all other cases, the corresponding sizes may be understood as hydrodynamic equivalent size-distributions, which in MWCNT may be due to signals from more than one particle dimension as well as the catalyst contaminants. The DLS data demonstrated that the dispersion was achieved and more detailed understanding of the MWCNTs characteristics can be observed from the TEM analyses (Fig. 1C). It appears that the dispersions of NM-400 produced the finest dispersion followed by NM-402, NM-403 and NRCWE-007. The coarsest dispersions were achieved for NM-401 and NRCWE-006. The results indicate that de-aggregation and dis-entanglement was less efficient for NM-401 and NRCWE-006 and moderate for NM-403, which shows major and secondary peak sizes in the range of 500 and 200 nm size, respectively. The PDI for the MWCNTs varied between 0.249 ± 0.020 (NM-401) and 0.707 ± 0.160 (NM-402), which reflect the apparent irregular broad or multimodal size-distribution of these NMs. PDI-values above 0.7 are usually considered not suitable for sizing by the DLS manufacturer (http://www.malvern.com/common/downloads/campaign/MRK1764-01.pdf).

The hydrodynamic size-distribution of the benchmark ZnO, NM-110, is also shown in Fig. 1a. The NM-110 is observed with a relatively broad monomodal peak with a peak size at 190 nm and a minor fraction reaching into the nanosize-range. NM-110, therefore, clearly has a larger particle size in the dispersion medium than both the $TiO_2$ and SAS NMs. The PDI for NM-110 was 0.091 ± 0.031.

### 3.3. Characterization of the exposure media

The results from the agglomeration and sedimentation studies in the exposure media are shown in Fig. 2. Based on the variation in relative intensity, extensive sedimentation was observed after

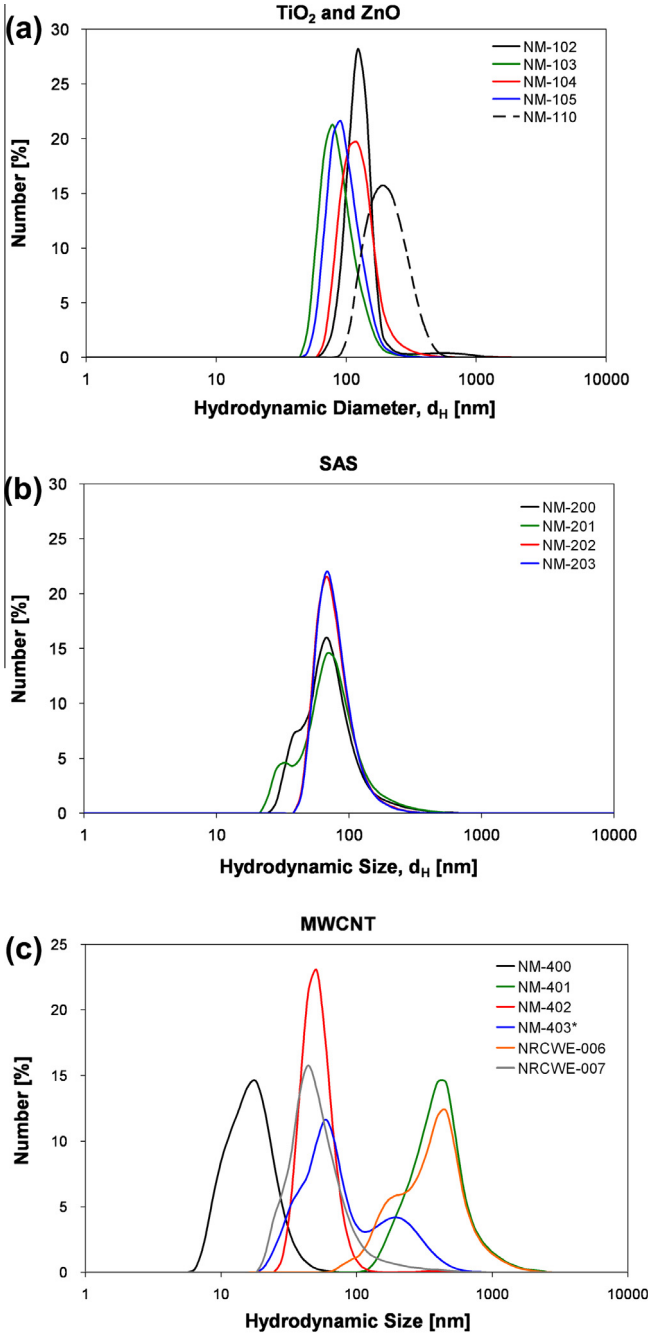


**Fig. 1.** Hydrodynamic number size-distributions of the batch dispersions prepared by using the dispersion protocol. (a) Size-distribution of all tested $TiO_2$ and the ZnO (NM-110) benchmark NM. (b) Size-distribution of the SAS. (c) Apparent hydrodynamic size-distribution of the dispersed MWCNTs samples. Due to a variable mathematical size-solution to the PCS, the size-distribution data for NM403* was the average of all the 12 first size spectra giving an overall repeatable size-distribution instead of the standard average of 6 analyses. Standard deviations in the analyses are not given for graphical reasons. Presence of smaller nanoparticles cannot be ruled out in these analyses due to potential masking effects by the coarser particles.

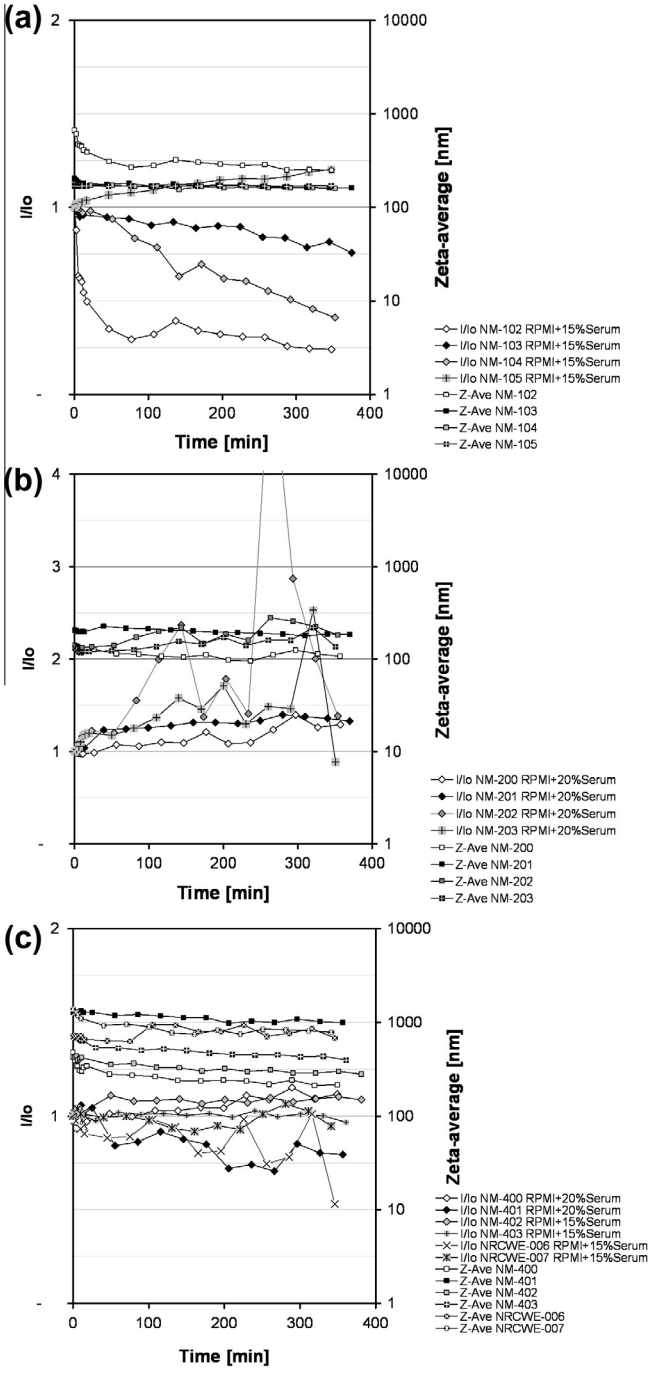


**Fig. 2.** Temporal evolution of the relative scattered light intensity ($I/I_o$) and average hydrodynamic Zeta-size (Z-Ave) for 0.256 mg/ml of: (a) $TiO_2$, (b) SAS, and (c) MWCNTs in RPMI added denoted 15% or 20% w/v fetal calf serum.

6 h in dispersions with NM-102 (ca. 75%), NM-104 (ca. 60%), NM103 (ca. 25%), NM-401 (ca. 25%) and NRCWE-006 (ca. 50%). Odd temporal variation was observed in experiments with NM-202, NM-203, and NRCWE-006, with one or more sequential increases and drops in relative intensity. The interpretation is that these dispersions are subject to slow sedimentation involving one or more accumulation events close to the bottom of the vials, where the intensity is measured. This also explains the increases in relative intensity observed in dispersions with NM-105 and all SAS; and to a lesser extend in dispersions with NM-400 and NM-402. Limited sedimentation appears to occur in the dispersions with NM-403 and NRCWE-007.

Combining the information from the temporal evolution in relative intensities and average Zeta-size reveals five different evolution patterns in the dispersions. (1) In NM-102, NM103, NM-400 and NM-401, sedimentation occurs in combination of fining, suggesting it is preferentially the coarsest particles that drop out of suspension. (2) In NM-103 there is a strong component of total sedimentation, which also appear to very dominant in the

dispersion with NM-104. (3) In NM-200, NM-201, NM-400, NM-402, and NRCWE-006, the suspensions are dominated by a combination of accumulation and fining/dissolution. We assume that the dissolution of these NM's would still be negligible to moderate in RPMI with 15–20% w/v fetal calf serum. Instead, it is interpreted as preferential loss of the coarser particles combined with accumulation of particles at the base of the test vial. (4) For NM-402, NM-403, and NRCWE-007, the temporal evolution is dominated by fining/dissolution with negligible change in relative intensity. As above, this is explained by preferential deposition of the coarsest particles; possibly sedimentation in combination with accumulation. (5) The last type of temporal evolution pattern was observed for NM-202 and NM-203, and to a much lesser degree in NM-105 where the Zeta-average increased during increase in relative intensity. This type of evolution is inferred to be due to slow deposition and accumulation at the vial bottom resulting in concentration-induced agglomeration. Possibly agglomeration alone can cause this relationship between size and scattered intensity.

It should be emphasized that all these sedimentation studies were completed at NM concentrations at the highest dose (256 μg/ml) tested. Lower doses would normally be associated with slower sedimentation and less interaction and agglomerate formation. Consequently, the reported observations should be considered the worst case.

### 3.4. In vitro micronucleus assay in human lymphocytes

The frequencies of micronucleated binucleate cells (MNBCs) and the cytokinesis-block proliferation indices (CBPI), obtained following lymphocytes exposure to nanosized $TiO_2$, SAS and MWCNTs, are presented in Figs. 3–5. Some variability in the vehicle

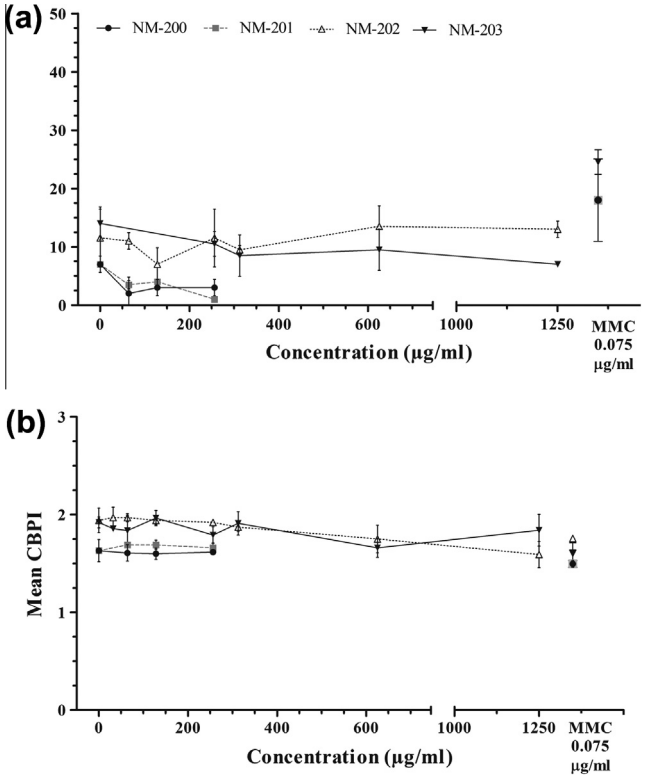


**Fig. 4.** Results from *in vitro* micronucleus assay after exposure to SAS: (a) Frequency of micronucleated binucleate cells (MNBCs) per 1000 binucleate cells (BC); (b) cytokinesis block proliferation index (CBPI). Results are expressed as Mean ± Standard Deviation. MMC data relative to each experiment are also presented ($p < 0.05$).

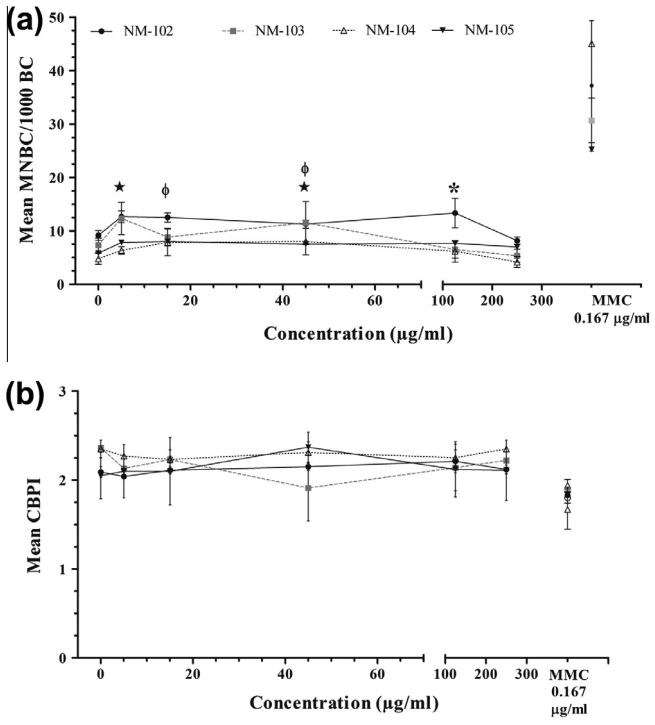


**Fig. 3.** Results from *in vitro* micronucleus assay after exposure to $TiO_2$: (a) Frequency of micronucleated binucleate cells (MNBCs) per 1000 binucleate cells (BC); (b) cytokinesis block proliferation index (CBPI). Results are expressed as Mean ± Standard Deviation. Significant differences in MNBCs frequency as compared to controls were observed for: ∗ NM-102, ★ NM-103 and Φ NM-104. MMC data relative to each experiment are also presented ($p < 0.05$).

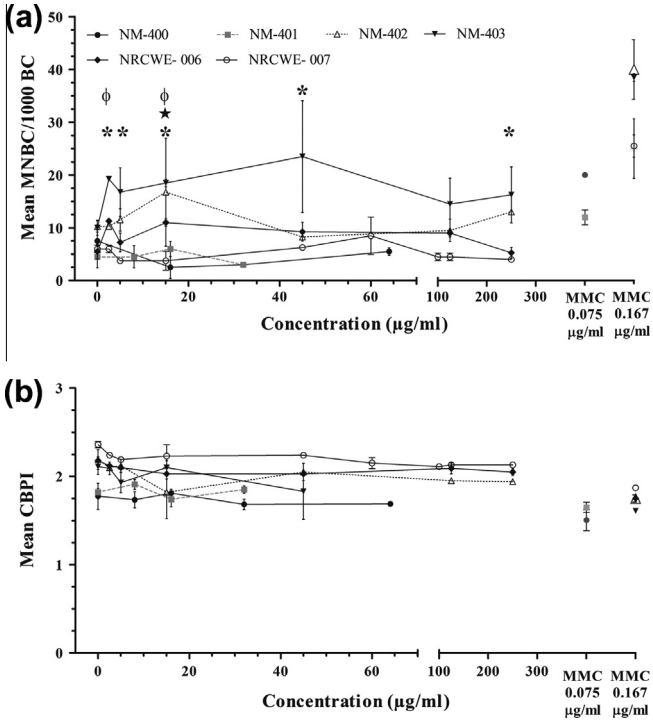


**Fig. 5.** Results from *in vitro* micronucleus assay after exposure to MWCNT: (a) Frequency of micronucleated binucleate cells (MNBCs) per 1000 binucleate cells (BC); (b) cytokinesis block proliferation index (CBPI). Results are expressed as Mean ± Standard Deviation. Significant differences in MNBCs as compared to controls were observed for: ∗ NM-403, ★ NM-402, Φ NRCWE-006. MMC data relative to each experiment are also presented ($p < 0.05$).

control data was noted, which is probably associated to inter- individual variability, given the fact that peripheral blood lymphocytes from several donors were used. However, it is noteworthy that the majority of the controls displayed a background frequency of MNBC within the mean ± standard deviation of our historical control data (7.07 ± 3.17).

Statistical comparison of the results between $TiO_2$ NM-exposed and vehicle-exposed lymphocytes showed significantly increased frequencies of MNBC for NM-102 at the dose of 125 μg/ml ($p = 0.038$), NM-103 at the doses of 5 and 45 μg/ml ($p = 0.007$ and 0.039) and NM-104 at 15 and 45 μg/ml ($p = 0.037$ and 0.048); no significant effect was observed for NM-105 (Fig. 3A). None of the tested $TiO_2$ NMs induced a dose-dependent effect, as evaluated by regression analysis. Cell viability and cell cycle progression, were assessed by the RI (data not shown) and by the CBPI values (Fig. 3B) and were not affected by any of the $TiO_2$ NMs treatments. The four SAS tested failed to induce significant increases in the frequency of MNBCs (Fig. 4) and did not affect the CBPI or the RI values, at the tested dose-range. Concerning MWCNTs (Fig. 5), significant increases in MNBC frequencies were detected after exposure to one dose of NM-402, 15 μg/ml ($p = 0.015$), to NRCWE-006 at 2.5 and 15 μg/ml ($p = 0.007$ and 0.009) and to all doses of NM-403 ($p < 0.018$) except at 125 μg/ml ($p = 0.083$). The remaining MWCNT did not induce micronuclei in human lymphocytes. Although NM-403 and NRCWE-006 displayed positive results, no dose-effect relationship was found by regression analysis. CBPI and RI were not significantly affected by any of the MWCNTs (Fig. 5B).

Considering the pooled data from all experiments, cells treatment with ZnO (64 μg/ml), which was included as a possible nanosized positive control, produced a slight yet significant increase in the mean frequency of MNBC/1000 BC (±standard deviation), from 8.01 ± 3.45 to 11.41 ± 4.15 ($p = 0.0016$). Furthermore, ZnO exposure caused a significant decrease in the CBPI value, as compared to the vehicle control, reflecting a delay in cell cycle progression related to cytotoxicity ($p = 0.046$). Based on this marginal (1.4-fold) effect, ZnO cannot be recommended as a nanosized positive control for the micronucleus assay in human lymphocytes. Overall, MMC treatment (0.167 μg/ml) resulted in a significant 3.8-fold increase in the frequency of MNBC, over the vehicle control ($p < 0.0001$), and also in a significant reduction of CBPI ($p < 0.001$).

Finally, amongst all the NMs analyzed, the frequency of micronucleated mononucleate cells (results not shown) was increased only by treatment with 45 μg/ml of NM-103 ($p = 0.013$).

## 4. Discussion

Toxicological information on NMs is of utmost importance for safety assessment, since NMs are already used in many consumer products and, e.g., in biomedicine and will have a number of new applications in the future. Many recent studies have addressed the genotoxicity of NMs, generating contradictory results and conclusions. Since these discrepancies probably relate to variations in NM characteristics, means of NM dispersion, cell systems, and the genotoxicity testing itself, the use of well characterized NMs, standardized dispersion methods, and validated genotoxicity tests seems to be crucial.

In the present study, we evaluated the genotoxicity of selected NMs most of which had been obtained under GLP and can serve as international benchmarks (Joint Research Centre repository). Using the cytokinesis-block micronucleus assay in human lymphocytes (OECD, 2010), we observed slight increases in the frequencies of MNBC for some $TiO_2$ NMs and MWCNTs, as compared to controls, but no clear monotonic dose-response relationships were obtained.

The results of the micronucleus assay with NM-103 and NM-104 suggest an *in vitro* genotoxic effect in human lymphocytes, considering that there were several statistically significant data points. NM-102 produced a single significant data point while NM-105 failed to induce micronuclei in the present conditions. Previous studies with human lymphocytes *in vitro* showed a dose-dependent induction of micronuclei by nanosized $TiO_2$ (50 and 100 μg/ml) similar to NM-105 (15% rutile, 85% anatase) (Kang et al., 2008). On the other hand, nanosized anatase (<25 nm), resembling NM-102, induced a dose-dependent increase in chromosomal aberrations at a similar dose-range (12.5–300 μg/ml) as tested in the present study (Catalán et al., 2012). However, the same nanosized anatase (20–200 μg/ml) did not induce DNA damage in human lymphocytes, as evaluated by the comet assay (Hackenberg et al., 2011a). Interestingly, the latter authors were able to detect, by TEM, $TiO_2$ particle aggregates in the cytoplasm of only 5 cells out of 100, which suggests that most lymphocytes did not efficiently take up $TiO_2$ anatase. If this is generally true, it is possible that the genotoxic effects observed in other studies have been indirectly mediated, e.g., by the influence of $TiO_2$ on lymphocyte membrane, by the monocytes (capable of phagocytosis) present in the cultures (Catalán et al., 2012), or by an unspecific effect of NMs on culture conditions. Poor uptake to lymphocytes may also explain the marginal genotoxic effect (1.4-fold) on micronucleus frequency of the partly soluble ZnO, which was considered in our study as a possible nanosized positive control based on earlier reports. In fact, ZnO has been described to induce a clear increase (4–5-fold) in micronucleated cells in human epithelial A549 and U87 glioma cells (Corradi et al., 2012; Wahab et al., 2011).

Published *in vitro* data with other human cell lines generally agree on the induction of micronuclei by uncoated nanosized $TiO_2$ anatase and on negative results for coated $TiO_2$ rutiles (Osman et al., 2010; Shukla et al., 2011; Wang et al., 2007). However, there does not appear to exist earlier studies on micronucleus induction by the coated rutiles NM-103 (hydrophobic, dimethicone-coated) and NM-104 (hydrophilic, glycerine-coated). In studies with human bronchial epithelial BEAS 2B cells, nanosized rutile ($10 \times 40$ nm) coated with amorphous $SiO_2$ and fine rutile (<5 μm) did not induce micronuclei, while nanosized $TiO_2$ anatase (10 nm and < 25 nm) and fine anatase (200 nm) did (Falck et al., 2009; Gurr et al., 2005). Interestingly, Rahman et al. (2002) reported that micronuclei induced by ultrafine $TiO_2$ ($\leqslant$20 nm; phase not specified) in Syrian hamster embryo SHE cells were kinetochore-negative and thereby due to a clastogenic effect. *In vivo*, nanosized $TiO_2$ (74% anatase with 26% brookite) did not affect the frequency of micronucleated polychromatic erythrocytes (PCEs) in mouse bone marrow after inhalation exposure (Lindberg et al., 2012) while another $TiO_2$ (75% anatase, 25% rutile) given in drinking water, elevated the level of micronucleated PCEs in mouse blood (Trouiller et al., 2009). Systemic $TiO_2$ doses were considerably higher in the oral than in the inhalation study (Lindberg et al., 2012), and Trouiller et al. (2009) explained their positive finding by a secondary genotoxic mechanism associated with inflammation.

In accordance with our negative results following SAS exposure, a previous study in human lymphocytes exposed to 15 or 55 nm SAS, found no induction of micronuclei (Downs et al., 2012). Nevertheless, oxidative DNA damage was observed in a comet assay with human lymphocytes *in vitro*, after exposure to 100 μg/ml of unmodified nanosized (10–50 nm) SAS but not after exposure to vinyl- or aminopropyl/vinyl-modified amorphous silica (Lankoff et al., 2012); none of the three forms of SAS was positive in the classical comet assay with lymphocytes, although flow cytometry suggested a gradual increase in cellular uptake of the NMs, reaching a plateau after 12–14 h. In Balb/3T3 mouse fibroblasts exposed to NM-200 or NM-203 (100 μg/ml), Uboldi et al. (2012) did not

detect micronucleus induction, although the NMs were internalized and accumulated in the cytoplasm. In A549 cells, none of three types of SAS (16, 60 and 104 nm) were able to significantly elevate the frequency of MNBC (Gonzalez et al., 2010). In contrast, together with the accumulation of SAS nanoparticles and aggregates in the cytoplasm of A549 cells, Mu et al. (2012) observed significant DNA damage by the comet assay, suggesting an indirect mechanism of action. Furthermore, SAS NMs (actual size 34 nm) induced micronuclei in 3T3-L1 mouse fibroblasts and mutations in mouse embryonic fibroblasts carrying the *lacZ* reporter gene, while smaller and larger particles (11 nm and 248 nm) did not (Park et al., 2011). In rats, intravenous injections at the maximum tolerated dose of SAS NMs (15 and 55 nm; 50 and 125 mg/kg b.wt) led to an increase in micronucleated reticulocytes and (for the 15 nm SAS) DNA damage in the liver, supposedly due to a secondary mechanism involving inflammation (Downs et al., 2012), a process which is not fully present in cell cultures.

In the present study, we observed clear micronucleus induction with two of the six MWCNTs examined. The thick (diameter 69 nm) and long (4423 nm) NRCWE-006, but also the thin (diameter 11 nm) and short (394.3 nm) NM-403 were positive. However, NRCWE-007 and NM-400, two other similarly thin (15 and 11 nm, respectively) and short (369 and 726 nm, respectively) MWCNTs, were negative. Therefore, differences observed in genotoxicity among closely related MWCNTs may not be simply explained by variation in tube length and diameter and other structural differences, including surface activity or transition metals present as impurities, might be implicated (Joint Research Centre, 2011; Lindberg et al., 2009). However, it is presently not clear how to predict which type of carbon nanotubes is actually harmful.

NM-402, yet another thin MWCNTs (11 × 1141 nm), yielded a positive response only at a single low dose (15 μg/ml), and the outcome was considered equivocal. Earlier studies reported that MWCNTs with dimensions of 20–40 × 1000–5000 nm (doses given in μl/ml, not comparable) and of 10–30 × 1000–2000 nm (50–300 μg/ml) were able to induce micronuclei and chromosomal aberrations in human lymphocytes (Cveticanin et al., 2010; Catalán et al., 2012). However, negative micronuclei results were also reported with MWCNTs of the same size (10–30 × 1000–2000 nm), following exposure of human lymphocytes to a single high dose of 1000 μg/ml, (Szendi and Varga, 2008); the same MWCNTs produced also negative data in BEAS 2B cells, although the NM was taken up by the cells (Lindberg et al., 2013).

It is of interest that NRCWE-006, that was positive in our study, is the same product that has previously been shown to induce mesothelioma after intraperitoneal injection in mice (3–3000 μg/animal) and rats (2 × 0.5 mg/animal) (Nagai et al., 2011; Takagi et al., 2008, 2012) and intrascrotal injection (1 mg/animal) in rats (Sakamoto et al., 2009). Fiber characterization indicated that NRCWE-006 was less flexible than NM-401, the other thick (63 nm) and long (3366 nm) MWCNT examined, which did not induce micronuclei. These results would fit the theory of Nagai et al. (2011) and Nagai and Toyokuni (2012), who recently suggested that MWCNTs with a diameter around 50 nm and high crystallinity (low flexibility) enter cells by piercing their membrane, are cytotoxic, and induce inflammation and mesothelioma, while MWCNTs with larger (~150 nm) or smaller (~2–20 nm) diameter are less effective. Studies with cell lines showed an increase in micronuclei after treatment with the same material as NRCWE-006 in A549 cells (20–200 μg/ml) (Kato et al., 2012) but not in Chinese hamster CHL/IU lung cells (tested up to toxic 5 μg/ml) (Asakura et al., 2010), although the latter study showed an increase in polyploidy and bi- and multinucleation. In RAW 264.7 mouse macrophages, both thick and long (149 × 5330 nm; 1–100 μg/ml) and thin and long (10–30 × 500–50 000 nm; 1–10 μg/ml) MWCNT induced micronuclei (Di Giorgio et al., 2011; Migliore et al., 2010). Micronuclei were also increased in rat lung epithelial RLE cells and human epithelial MCF-7 cells after treatment with MWCNT (10–50 μg/ml) with dimensions (11.3 × 700 nm) comparable to those of NM-400 (Muller et al., 2008); *in situ* hybridization revealed that the micronuclei in MCF-7 cells were induced by both clastogenic and aneugenic mechanisms. The latter MWCNT also produced micronuclei *in vivo* in type II pneumocytes of rats (2 mg/rat) after a single intratracheal instillation (Muller et al., 2008). Micronuclei were likewise increased in bone marrow PCEs of mice treated i.p. with thin and very long MWCNT (2–10 mg/kg b.wt; Ghosh et al., 2011) and with carboxylated and non-fuctionalized MWCNT (0.25–0.75 mg/kg b.wt; Patlolla et al., 2010). Other types of thin and long (10–15 × ~20 000 nm; 12.5–50 mg/kg b.wt) and thick (44 and 70 nm, no length given; 5–20 mg/kg b.wt) MWCNT did not induce MN in mouse bone marrow (Ema et al., 2012; Kim et al., 2011).

Under physiological conditions, the agglomeration process might play an important role in explaining the contradictions found in the literature, since agglomeration and thereby sedimentation of NMs seems to be time- and concentration-dependent. In BEAS 2B cells and malignant pleural mesothelioma MESO-1 cells, the intracellular dose of MWCNT depended on the dispersant used, and the level of cytotoxicity and inflammatory response correlated with the intracellular dose (Haniu et al., 2011). In our study, we used a standard procedure that was developed to ensure stable dispersion of the NMs, reducing agglomeration and subsequent sedimentation (Jensen et al., 2011). TEM and DLS analyses showed that nanosized particles were successfully obtained, although many agglomerates were still observable. An increasing size of the agglomerates with the dose might be responsible for the absence of a clear dose-response, especially in the case of NM-403. Similar difficulties were also reported by Lindberg et al. (2009), Ghosh et al. (2010), Hackenberg et al. (2011a). However, despite the possible interferences with the analysis, agglomeration is a natural behavior of nanosized particles, relevant in the assessment of their biological effects.

There is increasing evidence that similarities in, e.g., dimensions and surface to mass ratio within a group of NMs do not necessarily mean that such NMs are also similarly genotoxic. Regarding safety assessment, the differential genotoxicity observed for closely related NMs highlights the importance of investigating the toxic potential of each NM individually, instead of assuming a common mechanism and equal genotoxic effects for a set of similar NMs, before such assumption can be done with confidence. There is presently no consensus on testing protocols to be used for NMs, and no genotoxicity assays have specifically been validated for that purpose. Furthermore, very few comparative *in vivo* data are currently available to judge the performance of *in vitro* genotoxicity tests, and the mechanisms of genotoxic NMs are not well understood.

Overall, our findings contribute to the safety assessment of NMs, by increasing the weight of evidence in favor of the *in vitro* genotoxicity of some forms of nanosized $TiO_2$ and MWCNTs, and discarding a clastogenic or aneugenic effect of SAS in human lymphocytes. However, even with those forms of $TiO_2$ and MWCNTs that were positive in our study, the increases observed in micronuclei frequencies were small, and no clear dose-response relationships could be disclosed. Further ongoing assays, using other *in vitro* and *in vivo* systems to test the genotoxicity of the same NMs, together with more detailed information about their physicochemical characteristics, will improve the knowledge base for the evaluation of genotoxic risks associated with NMs and contribute to understanding the main characteristics that determine their toxicity, allowing a "safer-by-design" approach.

## Conflict of interest

The authors declare that there are no conflicts of interest.

## Disclaimer

This publication arises from the project NANOGENOTOX which has received funding from the European Union, in the framework of the Health Programme under Grant Agreement No. 2009 21. This publication reflects only the authors' views and the Executive Agency for Health and Consumers is not liable for any use that may be made of the information contained therein.

## Acknowledgements

The authors wish to thank Eleonora Paixão (INSA) for the support with the statistical analysis of the data and Yahia Kembouche (NRCWE) for conducting the DLS analysis.

## References

Asakura, M., Sasaki, T., Sugiyama, T., Takaya, M., Koda, S., Nagano, K., Arito, H., Fukushima, S., 2010. Genotoxicity and cytotoxicity of multi-wall carbon nanotubes in cultured Chinese hamster lung cells in comparison with chrysotile A fibers. J Occup. Health 52, 155–166.

Catalán, J., Järventaus, H., Vippola, M., Savolainen, K., Norppa, H., 2012. Induction of chromosomal aberrations by carbon nanotubes and titanium dioxide nanoparticles in human lymphocytes *in vitro*. Nanotoxicology 6, 825–836.

Corradi, S., Gonzalez, L., Thomassen, L.C., Bilaničová, D., Birkedal, R.K., Pojana, G., Marcomini, A., Jensen, K.A., Leyns, L., Kirsch-Volders, M., 2012. Influence of serum on in situ proliferation and genotoxicity in A549 human lung cells exposed to nanomaterials. Mutat. Res. 745, 21–27.

Cveticanin, J., Joksic, G., Leskovac, A., Petrovic, S., Sobot, A.V., Neskovic, O., 2010. Using carbon nanotubes to induce micronuclei and double strand breaks of the DNA in human cells. Nanotechnology 21, 015102.

De Temmerman, P.-J., Van Doren, E., Verleysen, E., Van der Stede, Y., Francisco, M.A.D., Mast, J., 2012. Quantitative characterization of agglomerates and aggregates of pyrogenic and precipitated amorphous silica nanomaterials by transmission electron microscopy. J. Nanobiotechnology 10 (24).

Di Giorgio, M.L., Di Bucchianico, S., Ragnelli, A.M., Aimola, P., Santucci, S., Poma, A., 2011. Effects of single and multiwalled carbon nanotubes on macrophages: cyto and genotoxicity and electron microscopy. Mutat. Res. 722, 20–31.

Downs, T.R., Crosby, M.E., Hu, T., Kumar, S., Sullivan, A., Sarlo, K., Reeder, B., Lynch, M., Wagner, M., Mills, T., Pfuhler, S., 2012. Silica nanoparticles administered at the maximum tolerated dose induce genotoxic effects through an inflammatory reaction while gold nanoparticles do not. Mutat. Res. 745 (1–2), 38–50.

EC-European Commission, 2012. COMMISSION RECOMMENDATION of 18 October 2011 on the definition of nanomaterial. <http://www.eur-lex.europa.eu/LexUriServ/LexUriServ.do?uri=OJ:L:2011:275:0038:0040:EN:PDF>.

Ema, M., Imamura, T., Suzuki, H., Kobayashi, N., Naya, M., Nakanishi, J., 2012. Evaluation of genotoxicity of multi-walled carbon nanotubes in a battery of in vitro and in vivo assays. Regul. Toxicol. Pharmacol. 63, 188–195.

Falck, G.C.-M., Lindberg, H.K., Suhonen, S., Vippola, M., Vanhala, E., Catalán, J., Savolainen, K., Norppa, H., 2009. Genotoxic effects of nanosized and fine $TiO_2$. Hum. Exp. Toxicol. 28, 339–352.

Ghosh, M., Bandyopadhyay, M., Mukherjee, A., 2010. Genotoxicity of titanium dioxide (TiO2) nanoparticles at two trophic levels: Plant and human lymphocytes. Chemosphere 81, 1253–1262.

Ghosh, M., Chakraborty, A., Bandyopadhyay, M., Mukherjee, A., 2011. Multi-walled carbon nanotubes (MWCNT): Induction of DNA damage in plant and mammalian cells. J. Hazard. Mater. 197, 327–336.

Gonzalez, L., Thomassen, L.C.J., Plas, G., Rabolli, V., Napierska, D., Decordier, I., Roelants, M., Hoet, P.H., Kirschhock, C.E.A., Martens, J.A., Lison, D., Kirsch-Volders, M., 2010. Exploring the aneugenic and clastogenic potential in the nanosize range: A549 human lung carcinoma cells and amorphous monodisperse silica nanoparticles as models. Nanotoxicology 4, 382–395.

Gonzalez, L., Sanderson, B.J.S., Kirsch-Volders, M., 2011. Adaptations of the in vitro MN assay for the genotoxicity assessment of nanomaterials. Mutagenesis 26, 185–191.

Gopalan, R., Osman, I., Amani, A., De Matas, M., Anderson, A., 2009. The effect of zinc oxide and titanium dioxide nanoparticles in the Comet assay with UVA photoactivation of human sperm and lymphocytes. Nanotoxicology 3, 33–39.

Guidi, P., Nigro, M., Bernardeschi, M., Scarcelli, V., Lucchesi, P., Onida, B., Mortera, R., Frenzilli, G., 2013. Genotoxicity of amorphous silica particles with different structure and dimension in human and murine cell lines. Mutagenesis 28, 171–180.

Guo, Y.Y., Zhang, J., Zheng, Y.F., Yang, J., Zhu, X.Q., 2011. Cytotoxic and genotoxic effects of multi-wall carbon nanotubes on human umbilical vein endothelial cells in vitro. Mutat. Res. 721, 184–191.

Gurr, J.R., Wang, A.S., Chen, C.H., Jan, K.Y., 2005. Ultrafine titanium dioxide particles in the absence of photoactivation can induce oxidative damage to human bronchial epithelial cells. Toxicology 213, 66–73.

Hackenberg, S., Friehs, G., Kessler, M., Froelich, K., Ginzkey, C., Koehler, C., Scherzed, A., Burghartz, M., Kleinsasser, N., 2011a. Nanosized titanium dioxide particles do not induce DNA damage in human peripheral blood lymphocytes. Environ. Mol. Mutagen. 52, 264–268.

Hackenberg, S., Scherzed, A., Technau, A., Kessler, M., Froelich, K., Ginzkey, C., Koehler, C., Burghartz, M., Hagen, R., Kleinsasser, N., 2011b. Cytotoxic, genotoxic and pro-inflammatory effects of zinc oxide nanoparticles in human nasal mucosa cells in vitro. Toxicol. in Vitro. 25, 657–663.

Haniu, H., Saito, N., Matsuda, Y., Kim, Y.-A., Park, K.-C., Tsukahara, T., Usui, Y., Aoki, K., Shimizu, M., Ogihara, N., Hara, K., Takanashi, S., Okamoto, M., Ishigaki, N., Nakamura, K., Kato, H., 2011. Effect of dispersants of multi-walled carbon nanotubes on cellular uptake and biological responses. Int. J. Nanomed. 6, 3295–3307.

ISO, 2004. Particle size analysis – Image analysis methods – Part 1: Static image analysis methods, in ISO 13322–1:2004. International Organization for Standardization, Geneva.

ISO, 2008. Representation of results of particle size analysis – Part 6: Descriptive and quantitative representation of particle shape and morphology, in ISO 9276–6:2008. International Organization for Standardization, Geneva.

Jensen, K.A., Kembouche, Y., Christiansen, E., Jacobsen, N.R., Wallin, H., Guiot, C., Spalla, O., Witschger, O., 2011. The generic NANOGENOTOX dispersion protocol – Standard Operation Procedure (SOP). NANOGENOTOX Deliverable Report No. 3: June 2011. <http://www.nanogenotox.eu>.

Jin, Y., Kannan, S., Wu, M., Zhao, J.X., 2007. Toxicity of luminescent silica nanoparticles to living cells. Chem. Res. Toxicol. 20, 1126–1133.

Joint Research Center (JCR), 2011. Impact of Engineered Nanomaterials on Health: Considerations for Benefit-Risk Assessment – EASAC Policy Report – Joint Research Centre Reference Report. Brussels: European Union. <http://www.publications.jrc.ec.europa.eu/repository/bitstream/111111111/22610/1/impact%20of%20engineered%20nanomaterials%20on%20health.pdf>.

Kang, S.J., Kim, B.M., Lee, Y.J., Chung, H.W., 2008. Titanium dioxide nanoparticles trigger p53-mediated damage response in peripheral blood lymphocytes. Environ. Mol. Mutagen. 49, 399–405.

Kato, T., Totsuka, Y., Ishino, K., Matsumoto, Y., Tada, Y., Nakae, D., Goto, S., Masuda, S., Ogo, S., Kawanishi, M., Yagi, T., Matsuda, T., Watanabe, M., Wakabayashi, K., 2012. Genotoxicity of multi-walled carbon nanotubes in both in vitro and in vivo assay systems. Nanotoxicology 7 (4), 452–461.

Kim, J.S., Lee, K., Lee, Y.H., Cho, H.S., Kim, K.H., Choi, K.H., Lee, S.H., Song, K.S., Kang, C.S., Yu, I.J., 2011. Aspect ratio has no effect on genotoxicity of multi-wall carbon nanotubes. Arch. Toxicol. 85, 775–786.

Krumbein, W.C., Sloss, L.L., 1963. Stratigraphy and Sedimentation. W.H, Freeman and Company, San Francisco.

Lankoff, A., Wegierek-Ciuk, A., Kruszewski, M., Lisowska, H., Banasik-Nowak, A., Rozga-Wijas, K., Wojewodzka, M., Slomkowski, S., 2012. Effect of surface modification of silica nanoparticles on toxicity and cellular uptake by human peripheral blood lymphocytes *in vitro*. Nanotoxicology. http://dx.doi.org/10.3109/17435390.2011.649796.

Lindberg, H.K., Falck, G.C., Suhonen, S., Vippola, M., Vanhala, E., Catalán, J., Savolainen, K., Norppa, H., 2009. Genotoxicity of nanomaterials: DNA damage and micronuclei induced by carbon nanotubes and graphite nanofibres in human bronchial epithelial cells in vitro. Toxicol. Lett. 186, 166–173.

Lindberg, H.K., Falck, G.C.-M., Catalán, J., Koivisto, A.J., Suhonen, S., Järventaus, H., Rossi, E., Nykäsenoja, H., Peltonen, Y., Alenius, H., Savolainen, K.M., Norppa, H., 2012. Genotoxicity of inhaled nanosized $TiO_2$ in mice. Mutat. Res. 745, 58–64.

Lindberg, H.K., Falck, G.C.-M., Järventaus, H., Suhonen, S., Vanhala, E., Catalán, J., Vippola, M., Savolainen, K.M., Norppa, H., 2013. Genotoxicity of single-wall and multi-wall carbon nanotubes in human epithelial and mesothelial cells in vitro. Toxicology. http://dx.doi.org/10.1016/j.tox.2012.12.008.

Malhi, G.S., 2012. The Chronic Toxicity of Titanium Dioxide Nanoparticles to the Freshwater Amphipod Hyalella azteca. Department of Biology. Waterloo, Ontario, Wilfrid Laurier University. Master of Science in Integrative Biology.

Mast, J., Demeestere, L., 2009. Electron tomography of negatively stained complex viruses: application in their diagnosis. Diag. Pathol. 4, 5.

Migliore, L., Saracino, D., Bonelli, A., Colognato, R., D'Errico, M.R., Magrini, A., Bergamaschi, A., Bergamaschi, E., 2010. Carbon nanotubes induce oxidative DNA damage in RAW 264.7 cells. Environ. Mol. Mutagen. 51, 294–303.

Muller, J., Decordier, I., Hoet, P.H., Lombaert, N., Thomassen, L., Huaux, F., Lison, D., Kirsch-Volders, M., 2008. Clastogenic and aneugenic effects of multi-wall carbon nanotubes in epithelial cells. Carcinogenesis 29, 427–433.

Mu, Q., Hondow, N.S., Krzemiński, L., Brown, A.P., Jeuken, L.J., Routledge, M.N., 2012. Mechanism of cellular uptake of genotoxic silica nanoparticles. Part. Fibre Toxicol. 23, 9–29.

Nagai, H., Toyokuni, S., 2012. Differences and similarities between carbon nanotubes and asbestos fibers during mesothelial carcinogenesis: shedding light on fiber entry mechanism. Cancer Sci. 103, 1378–1390.

Nagai, H., Okazaki, Y., Chew, S.H., Misawa, N., Yamashita, Y., Akatsuka, S., Ishihara, T., Yamashita, K., Yoshikawa, Y., Yasui, H., Jiang, L., Ohara, H., Takahashi, T., Ichihara, G., Kostarelos, K., Miyata, Y., Shinohara, H., Toyokuni, S., 2011. Diameter and rigidity of multiwalled carbon nanotubes are critical factors in mesothelial injury and carcinogenesis. Proc. Natl Acad. Sci. USA 108, E1330–1338.

Oberdörster, G., 2010. Safety assessment for nanotechnology and nanomedicine: concepts of nanotoxicology. J. Int. Med. 267, 89–105.

OECD – Organisation for Economic Co-operation and Development, 2010. OECD guideline for the testing of chemicals. In Vitro Mammalian Cell Micronucleus Test. Guideline 487.

Oesch, F., Landsiedel, R., 2012. Genotoxicity investigations on nanomaterials. Arch. Toxicol. 86, 985–994.

Osman, I.F., Baumgartner, A., Cemeli, E., Fletcher, J.N., Anderson, D., 2010. Genotoxicity and cytotoxicity of zinc oxide and titanium dioxide in HEp-2 cells. Nanomedicine 5, 1193–1203.

Park, M.V., Verharen, H.W., Zwart, E., Hernandez, L.G., van Benthem, J., Elsaesser, A., Barnes, C., McKerr, G., Howard, C.V., Salvati, A., Lynch, I., Dawson, K.A., de Jong, W.H., 2011. Genotoxicity evaluation of amorphous silica nanoparticles of different sizes using the micronucleus and the plasmid lacZ gene mutation assay. Nanotoxicology 5, 168–181.

Patlolla, A.K., Hussain, S.M., Schlager, J.J., Patlolla, S., Tchounwou, P.B., 2010. Comparative study of the clastogenicity of functionalized and nonfunctionalized multiwalled carbon nanotubes in bone marrow cells of Swiss-Webster mice. Environ. Toxicol. 25, 608–621.

Rahman, Q., Lohani, M., Dopp, E., Pemsel, H., Jonas, L., Weiss, D.G., Schiffmann, D., 2002. Evidence that ultrafine titanium dioxide induces micronuclei and apoptosis in Syrian hamster embryo fibroblasts. Environ. Health Perspect. 110, 797–800.

Sakamoto, Y., Nakae, D., Fukumori, N., Tayama, K., Maekawa, A., Imai, K., Hirose, A., Nishimura, T., Ohashi, N., Ogata, A., 2009. Induction of mesothelioma by a single intrascrotal administration of multi-wall carbon nanotube in intact male Fischer 344 rats. J. Toxicol. Sci. 34, 65–76.

Shukla, R.K., Sharma, V., Pandey, A.K., Singh, S., Sultana, S., Dhawan, A., 2011. ROS-mediated genotoxicity induced by titanium dioxide nanoparticles in human epidermal cells. Toxicol. in Vitro 25, 231–241.

Silva, M.J., Carothers, A., Dias, A., Luis, J.H., Piper, J., Boavida, M.G., 1994. Dose-dependence of radiation-induced micronuclei in cytokinesis-blocked human lymphocytes. Mutat. Res. 322, 117–128.

Singh, N., Manshian, B., Jenkins, G.J., Griffiths, S.M., Williams, P.M., Maffeis, T.G., Wright, C.J., Doak, S.H., 2009. NanoGenotoxicology: the DNA damaging potential of engineered nanomaterials. Biomaterials 30, 3891–3914.

Singh, C., Friedrichs, S., Levin, M., Birkedal, R., Jensen, K.A., Pojana, G., Wohlleben, W., Schulte, S., Wiench, K., Turney, T., Koulaeva, O., Marshall, D., Hund-Rinke, K., Kördel, W., Van Doren, E., De Temmerman, P-J., Francisco, M., Mast, J., Gibson, J., Koeber, N.R., Linsinger, T., Klein, C.L., 2011. NM-Series of Representative Manufactured Nanomaterials: Zinc Oxide NM-110, NM-111, NM-112, NM-113 Characterisation and Test Item Preparation. EUR 25066 EN – 2011.

Sycheva, L.P., Zhurkov, V.S., Iurchenko, V.V., Daugel-Dauge, N.O., Kovalenko, M.A., Krivtsova, E.K., Durnev, A.D., 2011. Investigation of genotoxic and cytotoxic effects of micro- and nanosized titanium dioxide in six organs of mice in vivo. Mutat. Res. 726, 8–14.

Szendi, K., Varga, C., 2008. Lack of Genotoxicity of Carbon Nanotubes in a Pilot Study. Anticancer Res. 28, 349–352.

Takagi, A., Hirose, A., Nishimura, T., Fukumori, N., Ogata, A., Ohashi, N., Kitajima, S., Kanno, J., 2008. Induction of mesothelioma in p53+/- mouse by intraperitoneal application of multi-wall carbon nanotube. J. Toxicol. Sci. 33, 105–116.

Takagi, A., Hirose, A., Futakuchi, M., Tsuda, H., Kanno, J., 2012. Dose-dependent mesothelioma induction by intraperitoneal administration of multi-wall carbon nanotubes in p53 heterozygous mice. Cancer Sci. 103, 1001–1004.

Trouiller, B., Reliene, R., Westbrook, A., Solaimani, P., Schiestl, R.H., 2009. Titanium dioxide nanoparticles induce DNA damage and genetic instability in vivo in mice. Cancer. Res. 69, 8784–8789.

Türkez, H., Geyikoğlu, F., 2007. An in vitro blood culture for evaluating the genotoxicity of titanium dioxide: the responses of antioxidant enzymes. 23, 19–23.

Uboldi, C., Giudetti, G., Broggi, F., Gilliland, D., Ponti, J., Rossi, F., 2012. Amorphous silica nanoparticles do not induce cytotoxicity, cell transformation or genotoxicity in Balb/3T3 mouse fibroblasts. Mutat. Res. 745, 11–20.

Wahab, R., Kaushik, N.K., Verma, A.K., Mishra, A., Hwang, I.H., Yang, Y.B., Shin, H.S., Kim, Y.S., 2011. Fabrication and growth mechanism of ZnO nanostructures and their cytotoxic effect on human brain tumor U87, cervical cancer HeLa, and normal HEK cells. J. Biol. Inorg. Chem. 16, 431–442.

Wang, J.J., Sanderson, B.J.S., Wang, H., 2007. Cyto- and genotoxicity of ultrafine $TiO_2$ particles in cultured human lymphoblastoid cells. Mutat. Res. 628, 99–106.

Wijnhoven, S.W.P., Dekkers, S., Hagens, W.I., de Jong, W.H., 2009. Exposure to nanomaterials in consumer products. RIVM Letter, Report 340370001/2009.

Zhu, L., Chang, D.W., Dai, L., Hong, Y., 2007. DNA damage induced by multiwalled carbon nanotubes in mouse embryonic stem cells. Nano Lett. 7, 3592–3597.